Inertia identification algorithm for high-performance speed control of electric motors

J.-W. Choi, S.-C. Lee and H.-G. Kim

Abstract: An estimation algorithm for identifying the moment of inertia, which is essential for the design of a high performance controller for a motor drive system, is presented. The proposed algorithm finds the moment of inertia by observing the position error signal generated by the speed observer, which contains error information on the moment of inertia. The proposed algorithm is easy to realise in an observer-based speed detection method. Simulation and experimental results are presented to confirm the performance of the moment of inertia estimation method, and show that the moment of inertia converges to an actual value within several speed changes. As a result, the speed control responses and designed speed controller performance match well.

1 Introduction

Recently, a need has arisen for a servo system that can combine a high-performance speed response capability with digital technology. This is due to the development of digital signal processors that can produce accurate computations within a short sampling time. Yet, to achieve high-performance speed control characteristics, fast and accurate speed detection is required. Currently, the MT method, which calculates the speed by counting the number of pulses generated by the encoder and the intervals between the pulses, is widely used for speed detection in many industrial applications [1, 2]. However, since this method only detects the average speed, it causes a detection lag time that degrades the speed response, especially in a low-speed region. Thus, speed detection methods using control theory have been investigated and found to produce a better speed detection performance than the MT method in a low-speed region [2–8].

Recent servo drives have adopted a serial encoder as a speed or position sensor instead of an incremental encoder, thereby allowing position information to be provided to the driver using serial communication. However, most serial encoders take several tens of microseconds to transfer the full position information to the control system. Therefore, if a serial encoder is used as a position sensor, the MT method cannot be applied to calculate the speed information, as a serial encoder does not output the pulses. In this case, speed detection methods using control theory are expected to be more promising.

Nevertheless, to obtain accurate speed information using a control theory-based speed detection method and carefully design the speed control characteristics, it is essential to know the system parameters, especially the moment of inertia [9–13]. Several methods have been already proposed to estimate the moment of inertia, for example, RELS (recursive extended least square) and the Kalman filter [10, 11]. Yet, since the gain matrix has to be tuned every sampling period to meet certain objective criteria, these methods are computationally intensive.

Accordingly, this paper proposes an algorithm for identifying the moment of inertia based on observing the position error signal generated by the speed observer that contains error information on the moment of inertia. Moreover, the proposed algorithm is easy to realise in an observer-based speed detection method. Simulation and experimental results are presented to confirm the performance of the moment of inertia estimation and speed control method, and the results show that the moment of inertia converges to an actual value within several speed changes.

2 Mechanical system modelling

The mechanical system is shown in Fig. 1 and the dynamic equations for the system are expressed by

$$J_m \frac{d\omega_m}{dt} + B_m\omega_m + T_d = T_e \tag{1}$$

$$\frac{d\theta_m}{dt} = \omega_m \tag{2}$$

where ω_m is the mechanical angular velocity, θ_m is the mechanical angular position, T_e is the driving torque, T_d is the disturbance load torque, J_m is the moment of inertia and B_m is the viscous damping coefficient. Although the speed information cannot be obtained directly from a position sensor, such as an encoder, the rotor speed is calculated by differentiating the rotor position, as in (2). The disturbance load torque is introduced as an augmented state variable,

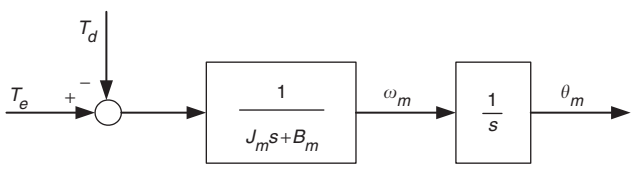

Fig. 1 *Model of mechanical system*

IEE Proceedings online no. 20050360

doi:10.1049/ip-epa:20050360

Paper first received 31st August and in final revised form 25th October 2005

The authors are with the School of Electronic & Electrical Engineering, Kyungpook National University, Sangyeok-dong, Buk-gu, Daegu 702-701, Korea

E-mail: jwchoi@ee.knu.ac.kr

and it is assumed that the load torque is a constant value and its derivative is zero, since a sampling frequency for the controller would be much higher than for a disturbance load torque variation. Thus

$$\frac{dT_d}{dt} = 0 \tag{3}$$

From (1)–(3), the dynamic state equations are given by

$$\frac{d\boldsymbol{x}}{dt} = \boldsymbol{A}\boldsymbol{x} + \boldsymbol{B}u, \quad y = \boldsymbol{C}\boldsymbol{x} \tag{4}$$

where

$$\boldsymbol{A} = \begin{bmatrix} 0 & 1 & 0 \\ 0 & -\frac{B_m}{J_m} & -\frac{1}{J_m} \\ 0 & 0 & 0 \end{bmatrix}, \quad \boldsymbol{B} = \begin{bmatrix} 0 \\ \frac{1}{J_m} \\ 0 \end{bmatrix},$$

$$\boldsymbol{C} = [\,1 \quad 0 \quad 0\,], \quad \boldsymbol{x} = \begin{bmatrix} \theta_m \\ \omega_m \\ T_d \end{bmatrix}, \quad u = T_e, \quad y = \theta_m$$

The input variable is the driving torque, the state variables are the mechanical angular position, mechanical angular velocity, and disturbance load torque, and the output variable is the mechanical angular position. Therefore, (4) can be rewritten as

$$\frac{d}{dt}\begin{bmatrix} \theta_m \\ \omega_m \\ T_d \end{bmatrix} = \begin{bmatrix} 0 & 1 & 0 \\ 0 & -\frac{B_m}{J_m} & -\frac{1}{J_m} \\ 0 & 0 & 0 \end{bmatrix}\begin{bmatrix} \theta_m \\ \omega_m \\ T_d \end{bmatrix} + \begin{bmatrix} 0 \\ \frac{1}{J_m} \\ 0 \end{bmatrix} T_e \tag{5}$$

3 Full-order state observer

When using the dynamic state equation in (4), a full order state [2, 5, 13] observer can easily be constructed by

$$\frac{d\hat{\boldsymbol{x}}}{dt} = \boldsymbol{A}\hat{\boldsymbol{x}} + \boldsymbol{B}u + \boldsymbol{K}(y - \boldsymbol{C}\hat{\boldsymbol{x}}) \tag{6}$$

where, the estimated state variables are $\hat{\boldsymbol{x}} = [\,\hat{\theta}_m \quad \hat{\omega}_m \quad \hat{T}_d\,]^T$ and the proportional gains are $\boldsymbol{K} = [\,k_1 \quad k_2 \quad k_3\,]^T$. Equation (6) can then be rewritten as

$$\frac{d}{dt}\begin{bmatrix} \hat{\theta}_m \\ \hat{\omega}_m \\ \hat{T}_d \end{bmatrix} = \begin{bmatrix} 0 & 1 & 0 \\ 0 & -\frac{B_m}{J_m} & -\frac{1}{J_m} \\ 0 & 0 & 0 \end{bmatrix}\begin{bmatrix} \hat{\theta}_m \\ \hat{\omega}_m \\ \hat{T}_d \end{bmatrix} + \begin{bmatrix} 0 \\ \frac{1}{J_m} \\ 0 \end{bmatrix} T_e + \begin{bmatrix} k_1 \\ k_2 \\ k_3 \end{bmatrix}(\theta_m - \hat{\theta}_m) \tag{7}$$

The proportional gains are chosen to achieve satisfactory dynamic characteristics of error, which are obtained by subtracting the observer in (6) from the real in (4), to produce the dynamic error equation

$$\frac{d\tilde{\boldsymbol{x}}}{dt} = (\boldsymbol{A} - \boldsymbol{K}\boldsymbol{C})\tilde{\boldsymbol{x}} \tag{8}$$

where, the error variable is defined by $\tilde{\boldsymbol{x}} = \boldsymbol{x} - \hat{\boldsymbol{x}}$. The characteristic equation is now given by

$$\det[s\boldsymbol{I} - (\boldsymbol{A} - \boldsymbol{K}\boldsymbol{C})] = s^3 + \left(k_1 + \frac{B_m}{J_m}\right)s^2 + \left(k_2 + k_1\frac{B_m}{J_m}\right)s - \frac{k_3}{J_m} = 0 \tag{9}$$

If $\boldsymbol{K}$ is chosen so that $\boldsymbol{A}-\boldsymbol{K}\boldsymbol{C}$ has stable and reasonably fast eigenvalues, then $\tilde{\boldsymbol{x}}$ will decay to zero and remain independent of the known forcing function $u(t)$ and its effect on state $\boldsymbol{x}(t)$ and irrespective of the initial condition $\tilde{\boldsymbol{x}}(0)$. $\hat{\boldsymbol{x}}(t)$ will then converge to $\boldsymbol{x}(t)$, regardless of the value of $\hat{\boldsymbol{x}}(0)$.

The selection of $\boldsymbol{K}$ is as follows. If the desired pole location of the estimator error is specified as α, β, γ, then the desired estimator characteristic equation is

$$s^3 - (\alpha + \beta + \gamma)s^2 + (\alpha\beta + \beta\gamma + \gamma\alpha)s - \alpha\beta\gamma = 0 \tag{10}$$

$\boldsymbol{K}$ can then be solved by comparing with the coefficients in (9) and (10), which gives

$$\begin{aligned} k_1 &= -(\alpha + \beta + \gamma) - \frac{B_m}{J_m} \\ k_2 &= (\alpha\beta + \beta\gamma + \gamma\alpha) + (\alpha + \beta + \gamma)\frac{B_m}{J_m} + \left(\frac{B_m}{J_m}\right)^2 \\ k_3 &= \alpha\beta\gamma J_m \end{aligned} \tag{11}$$

4 Moment of inertia identification

Since the estimated moment of inertia is different from the actual moment of inertia, J_m should be modified by $\hat{J}_m = J_m + \Delta J_m$. Similarly, actual viscous damping coefficient B_m should be modified by the estimated value $\hat{B}_m = B_m + \Delta B_m$. The physical and estimated state equations (5) and (7) are thus modified by

$$\frac{d}{dt}\begin{bmatrix} \theta_m \\ \omega_m \\ T_d \end{bmatrix} = \begin{bmatrix} 0 & 1 & 0 \\ 0 & -\frac{B_m}{J_m} & -\frac{1}{J_m} \\ 0 & 0 & 0 \end{bmatrix}\begin{bmatrix} \theta_m \\ \omega_m \\ T_d \end{bmatrix} + \begin{bmatrix} 0 \\ \frac{1}{J_m} \\ 0 \end{bmatrix} T_e \tag{12}$$

$$\frac{d}{dt}\begin{bmatrix} \hat{\theta}_m \\ \hat{\omega}_m \\ \hat{T}_d \end{bmatrix} = \begin{bmatrix} 0 & 1 & 0 \\ 0 & -\frac{\hat{B}_m}{\hat{J}_m} & -\frac{1}{\hat{J}_m} \\ 0 & 0 & 0 \end{bmatrix}\begin{bmatrix} \hat{\theta}_m \\ \hat{\omega}_m \\ \hat{T}_d \end{bmatrix} + \begin{bmatrix} 0 \\ \frac{1}{\hat{J}_m} \\ 0 \end{bmatrix} T_e + \begin{bmatrix} k_1 \\ k_2 \\ k_3 \end{bmatrix}(\theta_m - \hat{\theta}_m) \tag{13}$$

The error state variables are defined by the differences between the real and estimated state variables for the angle, speed and load torque, as in $\Delta\theta_m = \theta_m - \hat{\theta}_m$, $\Delta\omega_m = \omega_m - \hat{\omega}_m$, and $\Delta T_d = T_d - \hat{T}_d$, respectively. Laplace transforming (12) and (13) with zero initial conditions and subtracting (13) from (12) gives

$$s\Delta\theta_m(s) = \Delta\omega_m(s) - k_1\Delta\theta_m(s) \tag{14}$$

$$s\Delta\omega_m(s) = \left(\frac{1}{J_m} - \frac{1}{\hat{J}_m}\right)(T_e(s) - T_d(s)) - \frac{1}{\hat{J}_m}\Delta T_d(s) + \left(\frac{\hat{B}_m}{\hat{J}_m} - \frac{B_m}{J_m}\right)\omega_m(s) - \frac{\hat{B}_m}{\hat{J}_m}\Delta\omega_m(s) - k_2\Delta\theta_m(s) \tag{15}$$

$$s\Delta T_d(s) = -k_3\Delta\theta_m(s) \tag{16}$$

Substituting $T_e(s) - T_d(s) = (J_m s + B_m)\omega_m(s)$ in (15) gives

$$k_2\Delta\theta_m(s) = -\frac{1}{\hat{J}_m}\Delta T_d(s) + \left(\frac{\Delta J_m}{\hat{J}_m}s + \frac{\Delta B_m}{\hat{J}_m}\right)\omega_m(s) - \left(s + \frac{\hat{B}_m}{\hat{J}_m}\right)\Delta\omega_m(s) \quad (17)$$

And substituting $\Delta T_d(s) = -(k_3/s)\Delta\theta_m(s)$ from (16) in (17) then gives

$$\left(k_2 s - \frac{k_3}{\hat{J}_m}\right)\Delta\theta_m(s) = \left(\frac{\Delta J_m}{\hat{J}_m}s^2 + \frac{\Delta B_m}{\hat{J}_m}s\right)\omega_m(s) - \left(s^2 + \frac{\hat{B}_m}{\hat{J}_m}s\right)\Delta\omega_m(s) \quad (18)$$

Using $\omega_m(s) = s\theta_m(s)$ and $\Delta\omega_m(s) = (s + k_1)\Delta\theta_m(s)$ from (14), (18) can be rewritten as

$$\left(k_2 s - \frac{k_3}{\hat{J}_m}\right)\Delta\theta_m(s) = \left(\frac{\Delta J_m}{\hat{J}_m}s^3 + \frac{\Delta B_m}{\hat{J}_m}s^2\right)\theta_m(s) - \left(s^2 + \frac{\hat{B}_m}{\hat{J}_m}s\right)(s + k_1)\Delta\theta_m(s) \quad (19)$$

Finally, (19) can be expressed with respect to $\Delta\theta_m(s)$ and $\theta_m(s)$:

$$\left(s^3 + \left(k_1 + \frac{\hat{B}_m}{\hat{J}_m}\right)s^2 + \left(\frac{\hat{B}_m}{\hat{J}_m}k_1 + k_2\right)s - \frac{k_3}{\hat{J}_m}\right)\Delta\theta_m(s) = \left(\frac{\Delta J_m}{\hat{J}_m}s^3 + \frac{\Delta B_m}{\hat{J}_m}s^2\right)\theta_m(s) \quad (20)$$

Although it is assumed that ΔB_m is negligible, because the viscous damping coefficient is relatively small, the effect of ΔB_m is still extensively analysed in simulation studies. Thus (20) is reduced to

$$\left(s^3 + \left(k_1 + \frac{\hat{B}_m}{\hat{J}_m}\right)s^2 + \left(\frac{\hat{B}_m}{\hat{J}_m}k_1 + k_2\right)s - \frac{k_3}{\hat{J}_m}\right)\Delta\theta_m(s) = \left(\frac{\Delta J_m}{\hat{J}_m}s^3\right)\theta_m(s) \quad (21)$$

Equation (21) can be rewritten in a simpler form as

$$\Delta\theta_m(s) = \frac{\Delta J_m}{\hat{J}_m} \times \theta_{m\_hpf}(s) \quad (22)$$

where

$$\theta_{m\_hpf}(s) = \frac{s^3}{s^3 + (k_1 + \hat{B}_m/\hat{J}_m)s^2 + ((\hat{B}_m/\hat{J}_m)k_1 + k_2)s - (k_3/\hat{J}_m)}\theta_m(s) \quad (23)$$

where $\theta_{m\_hpf}(s)$ means the highpass filtered value for the angular position with the known gains and identified moment of inertia. $\theta_{m\_hpf}(s)$ reveals the relationship between the angular position error and the moment of inertia error. Once the known angular position and estimated angular position calculated from the full-order state observer have been established, the real moment of inertia can be calculated. Multiplying $\theta_{m\_hpf}(s)$ in (22) gives

$$\Delta\theta_m(s) \times \theta_{m\_hpf}(s) = \frac{\Delta J_m}{\hat{J}_m} \times \theta_{m\_hpf}(s)^2 \quad (24)$$

The actual moment of inertia can then be estimated by controlling $\Delta\theta_m(s) \times \theta_{m\_hpf}(s)$ to be zero. Block diagrams of the angular position, speed and disturbance torque observer, and the moment of inertia estimator are shown in Figs. 2 and 3. When controlling the error signal $\Delta\theta_m(s) \times \theta_{m\_hpf}(s)$ through the PI scheme, the moment of inertia is updated to the actual value. Figure 4 shows the speed controller when using the proposed moment of inertia estimator and full-order state observer.

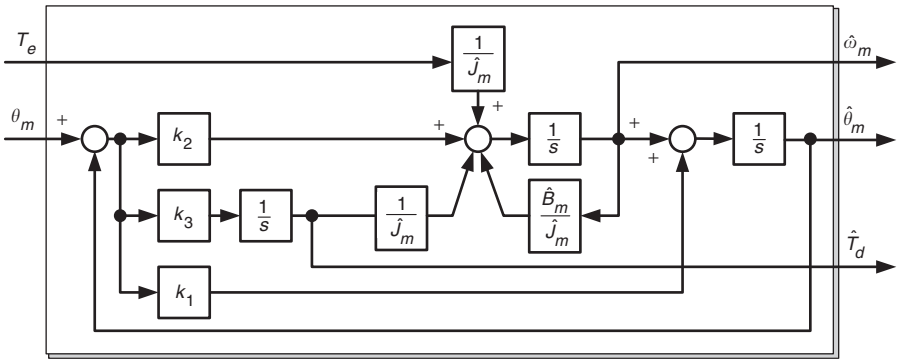

Fig. 2 *Full-order state observer with estimated moment of inertia*

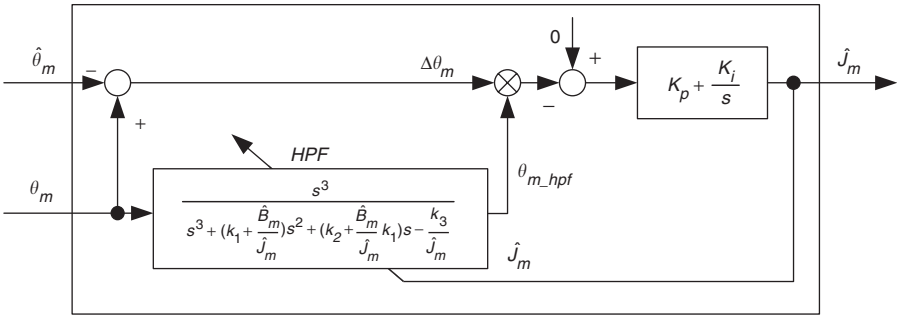

Fig. 3 *Moment of inertia estimator*

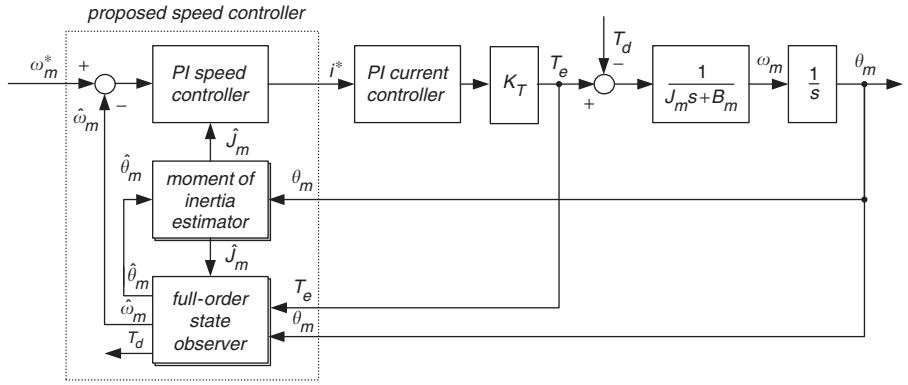

Fig. 4 *Speed controller with moment of inertia estimator and full-order state observer*

5 Simulation and experimental results

To verify the proposed control algorithm, a computer simulation was performed using the commercial software Matlab/Simulink. The cutoff frequency for the speed controller loop was chosen as $\omega_{sc} = 100\,\text{rad/s}$, and $K_{p\_sc} = \omega_{sc}\hat{J}_m/K_T$ and $K_{i\_sc} = 10\,K_{p\_sc}$ were the proportional and integral gains of the PI speed controller, respectively. Meanwhile, the triple poles for the full-order state observer were assigned at $\alpha = \beta = \gamma = -200\,\text{rad/s}$.

The feasibility of the proposed method was then verified based on an experiment performed with a 1 kW permanent magnet synchronous motor, TMS320C33 DSP control board, and three-phase PWM inverter composed of IGBTs. Figure 5 shows the overall experimental setup. In addition, an optical encoder with 2000 ppr was attached to measure the angular position through the MT method. Table 1 summarises the rated values and parameters of the permanent magnet synchronous motor utilised in the experiment.

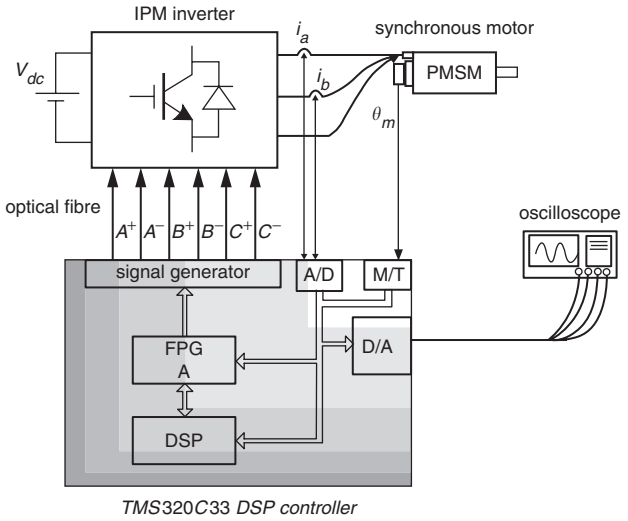

Fig. 5 *Experimental system setup*

5.1 Zero viscous damping system: $B_m = 0$

Figures 6 and 7 show the simulation and experimental results, respectively. The speed reference was changed based on a step function of +1000 and −1000 rpm. The estimated moment of inertia, reference speed, real speed, estimated speed and estimated speed error are shown from the top in the case of a detuned moment of inertia with −75 and +300% errors, respectively. In both cases, the estimated moment of inertia converged to the actual value within 2–5 speed changes and $K_p = 0.02$ and $K_i = 20$ were the proportional and integral gains of the PI controller, respectively, that were used to estimate the moment of inertia. Note that the convergence rate for the moment of inertia estimation in the −75% detuned case was faster than that for the +300% detuned case. The real speed in Fig. 7 was detected by the MT method.

When the estimated moment of inertia converged to the actual value, the speed response improved, demonstrating the effectiveness of the proposed method. However, the estimated speed had an overshoot with a smaller initial detuned moment of inertia value, yet an undershoot with a higher value. Nonetheless, the estimated speed errors converged to the actual value. However, the magnitude of the speed errors revealed a higher level of error with a smaller detuned value than with a larger detuned value. The simulation and experimental results showed similar response characteristics.

Table 1: Ratings and parameters of permanent magnet synchronous motor

Number of poles	8
Rated power	1 kW
Rated current	6.74 A RMS
Torque constant (K_T)	1.02975 Nm/A
Stator resistance (R_S)	0.704 Ω
Stator inductance (L_S)	7.996 mH
Moment of inertia(J_m)	0.00156 kgm^2

5.2 Non-zero viscous damping system: $B_m \neq 0$ and $0 \leq \hat{B}_m \leq 2\,B_m$

Figure 8–10 show the simulation results for the case of non-zero viscous damping coefficient which is assumed to be as large as a 25% of rated torque at rated speed, i.e. $B_m = 0.25 \times (T_c/\omega_m) = 0.0235\,\text{kgm}^2/\text{s}$. The viscous damping coefficient is non-zero and exactly known in advance, i.e. $\Delta B_m = 0$, as in Fig. 8. The estimated moment of inertia converged on the actual moment of inertia with a percentage error of −0.06%. The estimated moment of inertia converged to the actual value within two speed changes and $K_p = 0.1$ and $K_i = 100$ were the proportional and integral gains of the PI controller, respectively, which is five times higher than the previous simulation in Fig. 6.

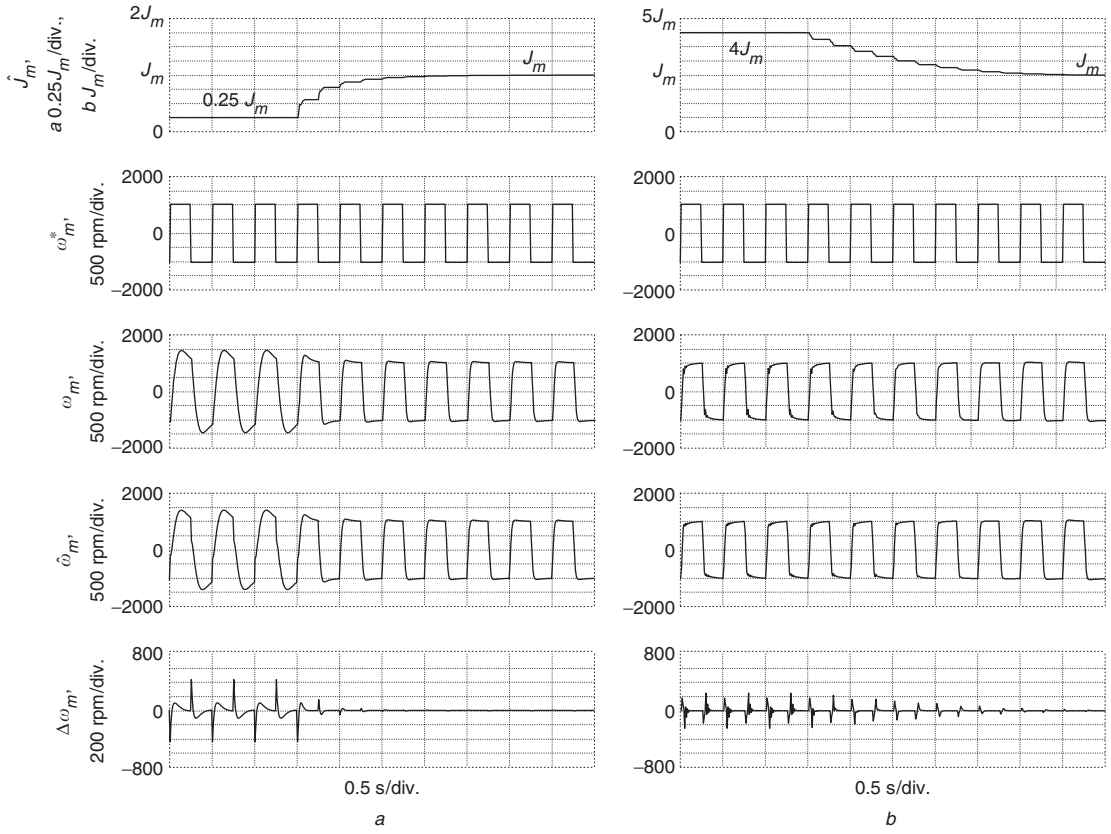

Fig. 6 *Simulation results for initial moment of inertial errors with $B_m = 0$*
a −75%
b +300%
From top: estimated moment of inertia, reference speed, real speed, estimated speed and estimated speed error

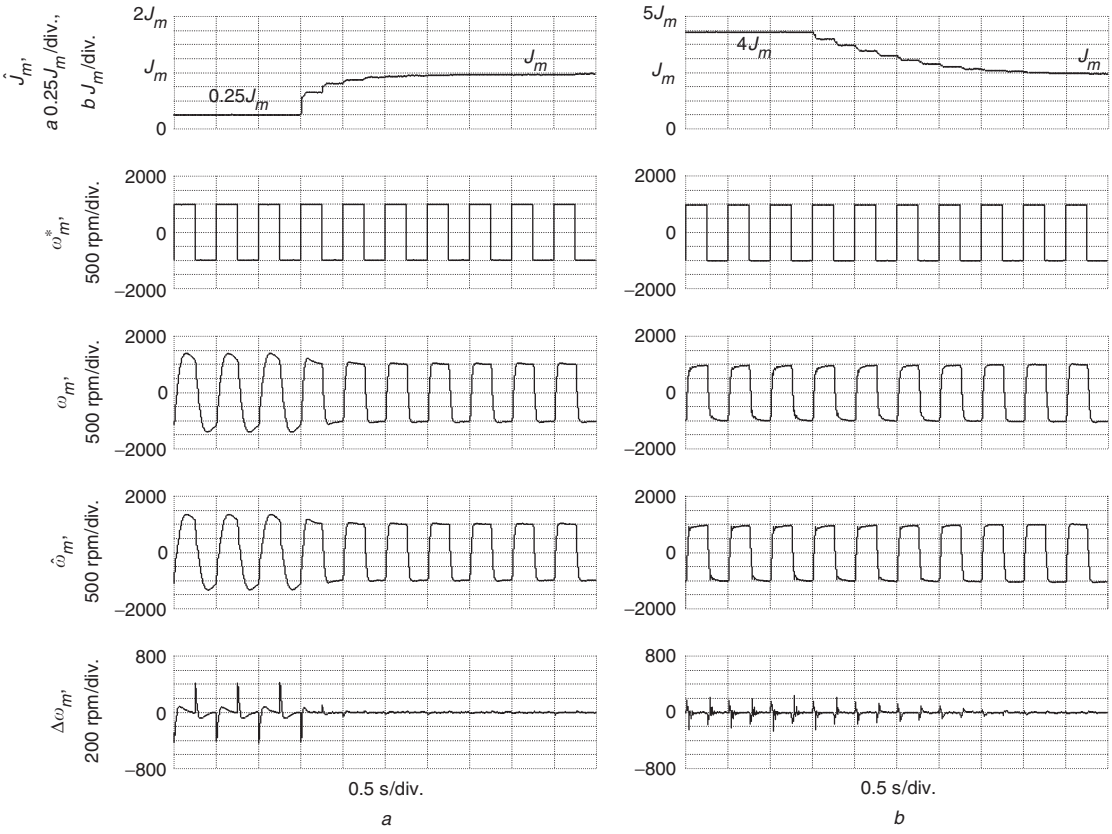

Fig. 7 *Experimental results for initial moment of inertia errors with $B_m = 0$*
a −75%
b +300%
From top: estimated moment of inertia, reference speed, real speed, estimated speed and estimated speed error

Fig. 8 *Simulation results for initial moment of inertia errors with known non-zero viscous damping coefficient* $\hat{B}_m = B_m \neq 0$
a −75%
b +300%
From top: estimated moment of inertia, reference speed, real speed, estimated speed and estimated speed error

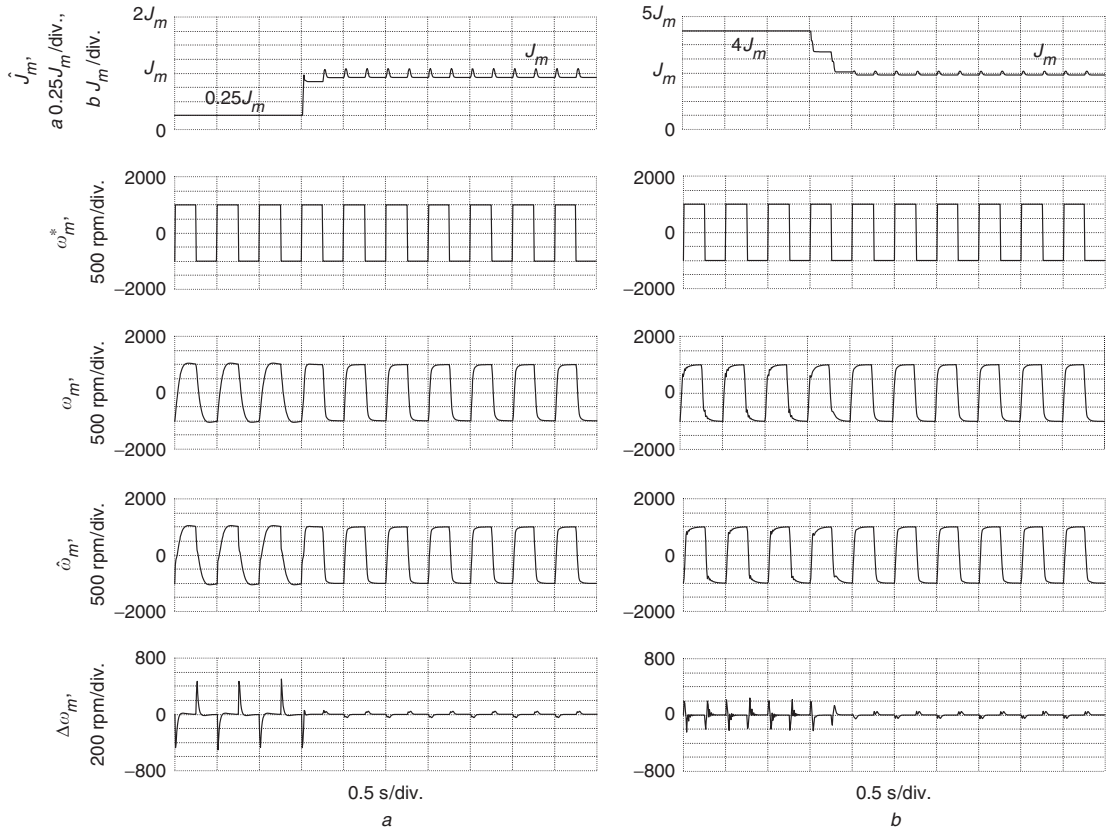

Fig. 9 *Simulation results for initial moment of inertia errors with unknown non-zero viscous damping coefficient* $\hat{B}_m = 0$
a −75%
b +300%
From top: estimated moment of inertia, reference speed, real speed, estimated speed and estimated speed error

Fig. 10 *Simulation results for initial moment of inertia errors with unknown non-zero viscous damping coefficient* $\hat{B}_m = 2B_m$
a −75%
b +300%
From top: estimated moment of inertia, reference speed, real speed, estimated speed and estimated speed error

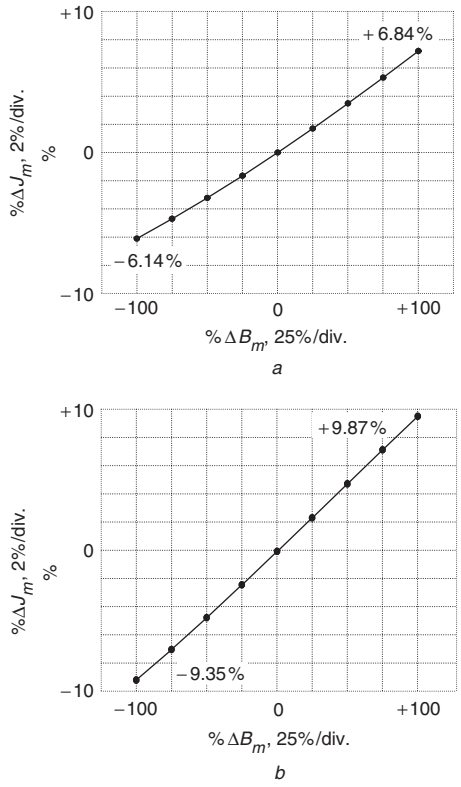

Fig. 11 *Percentage errors of the estimated moment of initial for initial moment of inertia*
a −75%
b +300%

In the sequel the higher gains enhance convergence performance of parameter estimation.

However, in a practical system it is difficult to know the exact value, i.e. $\Delta B_m \neq 0$. Figures 9 and 10 show the simulation results with −100% and +100% errors in viscous damping coefficient. The error level of estimated moment of inertia is within ±7% for the case of −100% viscous damping coefficient at $K_p = 0.06$ and $K_i = 60$, also ±10% errors for the case of +100% viscous damping coefficient at $K_p = 0.08$ and $K_i = 80$. Figure 11 shows the percentage errors of the estimated moment of inertia with unknown viscous damping coefficient from −100 to +100% errors. As such, it is reasonable to conclude that the proposed algorithm operates well in a non-zero damping coefficient system.

6 Conclusions

This paper has presented an algorithm for estimating the moment of inertia. The proposed estimation algorithm finds the moment of inertia by observing the position error signal generated by the speed observer, which contains error information on the moment of inertia. Simulation and experimental results confirm the performance of the moment of inertia estimation method and show that a moment of inertia converges to the actual value within several speed changes, thereby allowing the speed PI controller to be well tuned to give the best performance designed by the user. The proposed algorithm renders the error level of estimated moment of inertia less than 10% (or 7%), even for the case with +100% (or −100%) viscous

damping errors of the parameter estimator and full-order state observer. Moreover, the proposed algorithm is easy to realise in an observer-based speed estimation method. This kind of an online moment of inertia estimation scheme for tuning the controller is especially recommended for a rotational moving system such as a high-precision spindle drive with high gains and proper speed excitation. Potentially, the application area can be extended to a robot system with a position dependent moment of inertia variation and an operation condition dependent moment of inertia changing system.

7 Acknowledgment

This work was supported by the Korean Research Foundation grant funded by the Korean Government (MOEHRD) (R08-2003-000-10906-0).

8 References

1 Ohmae, T., Matsuda, T., Kamiyama, K., and Tachikawa, M.: 'A microprocessor-controlled high- accuracy wide-range speed regulator for motor drives', *IEEE Trans. Ind. Electron.*, 1982, **29**, (3), pp. 207–211
2 Sul, S.-K.: 'Control of electric machinery' (Brain Korea, 2002), pp. 96–104
3 Lorenz, R.D., and Van Patten, K.W.: 'High-resolution velocity estimation for all-digital, ac servo drives', *IEEE Trans. Ind. Appl.*, 1991, **27**, (4), pp. 701–705
4 Fujita, K., and Sado, K.: 'Instantaneous speed detection with parameter identification for ac servo systems', *IEEE Trans. Ind. Appl.*, 1992, **28**, (4), pp. 864–872
5 Kim, H.-W., and Sul, S.-K.: 'A new motor speed estimator using Kalman filter in low speed range', *IEEE Trans. Ind. Electron.*, 1996, **43**, (4), pp. 498–504
6 Song, S.-H., and Sul, S.-K.: 'An instantaneous speed observer for low speed control of AC machine'. Proc. APEC, 1998, pp. 581–586
7 Kweon, T.-J., and Hyun, D.-S.: 'High- performance speed control of electric machine using low precision shaft encoder', *IEEE Trans. Power Electron.*, 1999, **14**, (5), pp. 838–849
8 Yang, S.-M., and Ke, S.-J.: 'Performance evaluation of a velocity observer for accurate velocity estimation of servo motor drives', *IEEE Trans. Ind. Appl.*, 2000, **36**, (1), pp. 98–104
9 Awaya, I., Kato, Y., Miyake, I., and Ito, M.: 'New motion control with inertia identification function using disturbance observer'. Proc. IECON, 1992, pp. 77–81
10 Kim, N.-J., Moon, H.-S., and Hyun, D.-S.: 'Inertia identification for the speed observer of the low speed control of induction machines', *IEEE Trans. Ind. Appl.*, 1996, **32**, (6), pp. 1371–1379
11 Hong, S.-J., Kim, H.-W., and Sul, S.-K.: 'A novel inertia identification method for speed control of electric machine'. Proc. IECON, 1996, pp. 1234–1239
12 Guo, Y., Huang, L., Qiu, Y., and Muramatsu, M.: 'Inertia identification and auto-tuning of induction motor using MRAS'. Proc. PIEMC, 2000, pp. 1006–1011
13 Lee, K.B., Yoo, J.Y., Song, J.H., and Choy, I.: 'Improvement of low speed operation of electric machine with an inertia identification using ROELO', *IEE Proc., Electro. Power Appl.*, 2004, **151**, (1), pp. 116–120